Journal of Power Sources 242 (2013) 222–229

Contents lists available at SciVerse ScienceDirect

Journal of Power Sources

journal homepage: www.elsevier.com/locate/jpowsour

# Single-crystalline $Li_4Ti_5O_{12}$ nanorods and their application in high rate capability $Li_4Ti_5O_{12}/LiMn_2O_4$ full cells

Liu Jiang Xi [a], Hong Kang Wang [a], Shi Liu Yang [a], Ru Guang Ma [a], Zhou Guang Lu [b], Chen Wei Cao [a], Kwan Lan Leung [a], Jian Qiu Deng [c], Andrey L. Rogach [a], C.Y. Chung [a,*]

[a] Department of Physics and Materials Science, City University of Hong Kong, Hong Kong Special Administrative Region
[b] South University of Science and Technology of China, Shenzhen, PR China
[c] School of Material Science and Engineering, Guilin University of Electronic Technology, Guilin 541004, China

## HIGHLIGHTS

- A simple method was used to fabricate single-crystalline $Li_4Ti_5O_{12}$ nanorods.
- $Li_4Ti_5O_{12}$ nanorods revealed higher capacity and more excellent rate capability.
- $Li_4Ti_5O_{12}$ nanorods possessed long cycling lifespan at high rate.
- $Li_4Ti_5O_{12}/LiMn_2O_4$ full cells displayed superior cycle stability.

## ARTICLE INFO

*Article history:*
Received 5 December 2012
Received in revised form
28 February 2013
Accepted 6 April 2013
Available online 29 April 2013

*Keywords:*
Lithium titanate
Nanorods
Lithium ion battery
High rate capability
Long lifespan

## ABSTRACT

Single-crystalline $Li_4Ti_5O_{12}$ nanorods have been successfully prepared through a molten salt method, followed by a precipitation method, and characterized with X-ray powder diffractometry, field-emission scanning electron microscopy, and transmission electron microscope. Their electrochemical properties have been studied by charge/discharge cycling and cyclic voltammetry. The results show that the single-crystalline $Li_4Ti_5O_{12}$ nanorods reveal high capacity, excellent rate capability and cycle stability. The discharge capacity up to 176.4 mAh $g^{-1}$ at 0.1 C rate is achieved. When tested at 10 C rate, the first discharge capacity reaches 135.9 mAh $g^{-1}$, and the capacity retention is more than 61.5% after 1500 cycles. Furthermore, high rate capability $Li_4Ti_5O_{12}/LiMn_2O_4$ full cells have been made using $Li_4Ti_5O_{12}$ nanorods as the negative electrode, which display superior cycle stability at high rate. The discharge capacity and the mass energy density sequentially reach 40 mAh $g^{-1}$ and 86.4 Wh $kg^{-1}$ at 10 C rate, while the capacity retention is about 60% after 1000 cycles.



## 1. Introduction

Rechargeable lithium ion batteries (LIBs) have been increasingly applied as power sources for electric vehicles (EV) and hybrid electric vehicles (HEV). The improvement of safety and cycling lifespan of LIBs for EV and HEV is an extremely attractive and challenging topic. Graphite, a commonly used anode material, has large volume variation of ~9% in the lithium insertion-extraction process, as well as severe safety issues due to dendritic lithium growth for its low operating voltage. Spinel $Li_4Ti_5O_{12}$ is considered to be a promising alternative anode material to graphite because of its better cycling lifespan and safety performance. The spinel structure of $Li_4Ti_5O_{12}$ offers a steady three-dimensional interstitial 8a tetrahedral and 16c octahedral space, allowing the intercalation of Li ions into the $Li_4Ti_5O_{12}$ framework and forming a rock-salt-type $Li_7Ti_5O_{12}$ structure [1]. The difference of lattice parameters between spinel and rock-salt phase is less than 0.1% [2], which results in excellent stability under electrochemical cycling. Moreover, this material has a stable voltage plateau at approximately 1.55 V vs. $Li^+/Li$, which prevents the reduction reaction of the electrolyte and the deposition of metallic lithium, which improves the safety. However, the electrodes made from untreated $Li_4Ti_5O_{12}$ usually show poor rate performance because of its poor electronic conductivity [3–5].

Various strategies have been exploited to improve the electrical conductivity of $Li_4Ti_5O_{12}$ anode material, such as nanostructuring [6–19], doping [20–26], surface coating [5,27–37], and so on. A one-pot template-free solvothermal synthesis of crystalline

* Corresponding author. Tel.: +852 34427835; fax: +852 34420538.
*E-mail address:* appchung@cityu.edu.hk (C.Y. Chung).

0378-7753/$ – see front matter © 2013 Elsevier B.V. All rights reserved.
http://dx.doi.org/10.1016/j.jpowsour.2013.04.020

$Li_4Ti_5O_{12}$ nanostructures was introduced, and the as-synthesized crystalline nanostructures showed good lithium intercalation/deintercalation performances at high rates (up to 30 C) and good cycling stabilities [13]. A sol–gel approach was developed to synthesize $Li_{3.9}Sn_{0.1}Ti_5O_{12}$ anode material by doping $Li_4Ti_5O_{12}$ particles with $Sn^{2+}$, and the specific capacities of the doped $Li_{3.9}Sn_{0.1}Ti_5O_{12}$ were much higher than the corresponding values of neat $Li_4Ti_5O_{12}$ when discharged at high current densities [21]. The $Li_4Ti_5O_{12}$ negative electrode was successfully prepared by a simple block copolymer assembly route, which had a reversible capacity of 115 mAh $g^{-1}$ with 90% capacity retention after 500 cycles at 10 C rate [32].

$Li_4Ti_5O_{12}$ materials of some specific morphologies are beneficial for rate capability, such as nanotubes [38], nanowires [39], nanosheets [40,41], nanorods [42], nanoplatelets [43], nanofibers [44], hollow spheres [45,46], porous structure [47–52], etc. The large scale production of one-dimensional $Li_4Ti_5O_{12}$ nanowires was achieved by firing a mixture of Li acetate and $TiO_2$ nanowires, which demonstrated superior rate capability even at 10 C rate [39]. Hierarchical structured $Li_4Ti_5O_{12}$ was fabricated by a hydrothermal route and the subsequent calcination, which displayed high discharge capacity of 128 mAh $g^{-1}$ at the high current density of 2000 mA $g^{-1}$ [40]. Spinel $Li_4Ti_5O_{12}$ with hollow-sphere structure was fabricated by a sol–gel process using carbon spheres as templates, and showed high lithium storage capacity, especially at high current rates [45]. The $Li_4Ti_5O_{12}$ mesoporous spheres exhibited superior high-rate performance of 114 mAh $g^{-1}$ at 30 C and good capacity retention of 125 mAh $g^{-1}$ after 200 cycles at 20 C, which is promising for high-rate lithium ion batteries [48]. Hierarchically porous $Li_4Ti_5O_{12}$ microspheres assembled by well-crystalline nanoparticles showed high coulombic efficiency, ultrahigh rate capability at high rates, and excellent capacity retention over 200 cycles [51].

In this study, we synthesized single-crystalline $Li_4Ti_5O_{12}$ nanorods using a molten salt method, followed by a precipitation method. The electrochemical performance of $Li_4Ti_5O_{12}$ nanorods was studied and compared with $Li_4Ti_5O_{12}$ nanoparticles, which revealed that the $Li_4Ti_5O_{12}$ nanorods have better rate capability and cycle stability. Furthermore, high rate capability $Li_4Ti_5O_{12}/LiMn_2O_4$ full cells have been made and investigated using $Li_4Ti_5O_{12}$ nanorods as the negative electrode.

## 2. Experiment procedures

### 2.1. Sample preparation

All chemicals were of analytical grade and used as received. $Li_4Ti_5O_{12}$ nanorods were synthesized using $Na_2TiO_3$ nanowires as the initial template, as shown in Fig. 1. The $Na_2TiO_3$ nanowires were synthesized by the alkaline hydrothermal process as reported elsewhere [53]. The $Li_2TiO_3$ nanowires were prepared by the sodium/lithium ion exchange in molten salts of $LiNO_3$ (88% mol) and LiCl (12% mol) at 450 °C for 2 h $Li_2TiO_3$ nanowires and $Ti(OC_4H_9)_4$ with the mole ration of 2:3 were dispersed into isopropanol under vigorous stirring for 4 h. Distilled water was added to precipitate $Ti^{4+}$ ions, followed by stirring for 2 h. The precipitate was collected and washed with absolute ethanol for several times. Powders obtained were dried in vacuum and calcined at 850 °C in atmospheric condition for 15 h. For comparison, $Li_4Ti_5O_{12}$ nanoparticles were prepared as follows. $TiO_2$ powders (Degussa P25) were mixed with $LiOH\cdot H_2O$ with the molar ratio of 5:4.3, dispersed into 2 mL ethanol, ground to form a fine mixture, dried at room temperature, and calcined at 850 °C in atmospheric condition for 15 h.

The cathode material $LiMn_2O_4$ were prepared as porous spheres, as in our previous report [54]. In a typical synthesis, $MnSO_4\cdot H_2O$ and $Na_2S_2O_8$ were mixed in distilled water at room temperature,

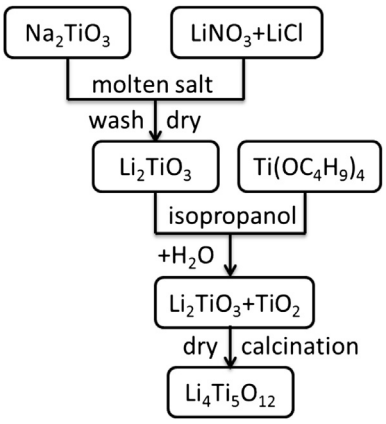


**Fig. 1.** Schematic diagram of the formation process of $Li_4Ti_5O_{12}$ nanorods.

and $AgNO_3$ solution was added. After the homogeneous solution was settled for 2 days at room temperature, the precipitate was collected and dried in a vacuum. Resulting powder was mixed with $LiOH\cdot H_2O$ with the molar ratio of 1.2:2, dispersed into 2 mL ethanol, ground to form a fine mixture, dried at room temperature, and finally calcined at 800 °C in atmospheric condition for 10 h.

### 2.2. Characterization of as-prepared samples

The crystalline structures of as-prepared products were characterized by X-ray diffraction (XRD) technique using a Siemens X-ray diffractometer with Cu Kα radiation. The morphologies of the as-prepared products were examined by a field-emission SEM (Hitachi S4800) and transmission electron microscopy (JEM-2100).

### 2.3. Electrochemical performance measurement

The electrochemical properties of the products were analyzed by making CR2032 coin-type cells. The anode and cathode slurries were separately prepared by mixing the active material, acetylene black and polyvinylidene fluoride (PVDF) in the weight ratio of 80:10:10 and 70:10:10. The blended anode and cathode slurries were then separately cast onto copper and aluminum foil current

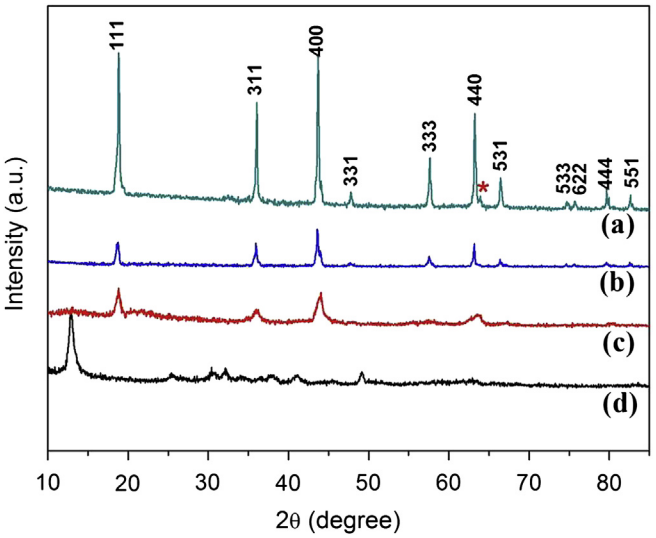


**Fig. 2.** The XRD patterns of (a) $Li_4Ti_5O_{12}$ nanorods; (b) $Li_4Ti_5O_{12}$ nanoparticles; (c) $Li_2TiO_3$ nanowires; (d) $Na_2TiO_3$ nanowires.

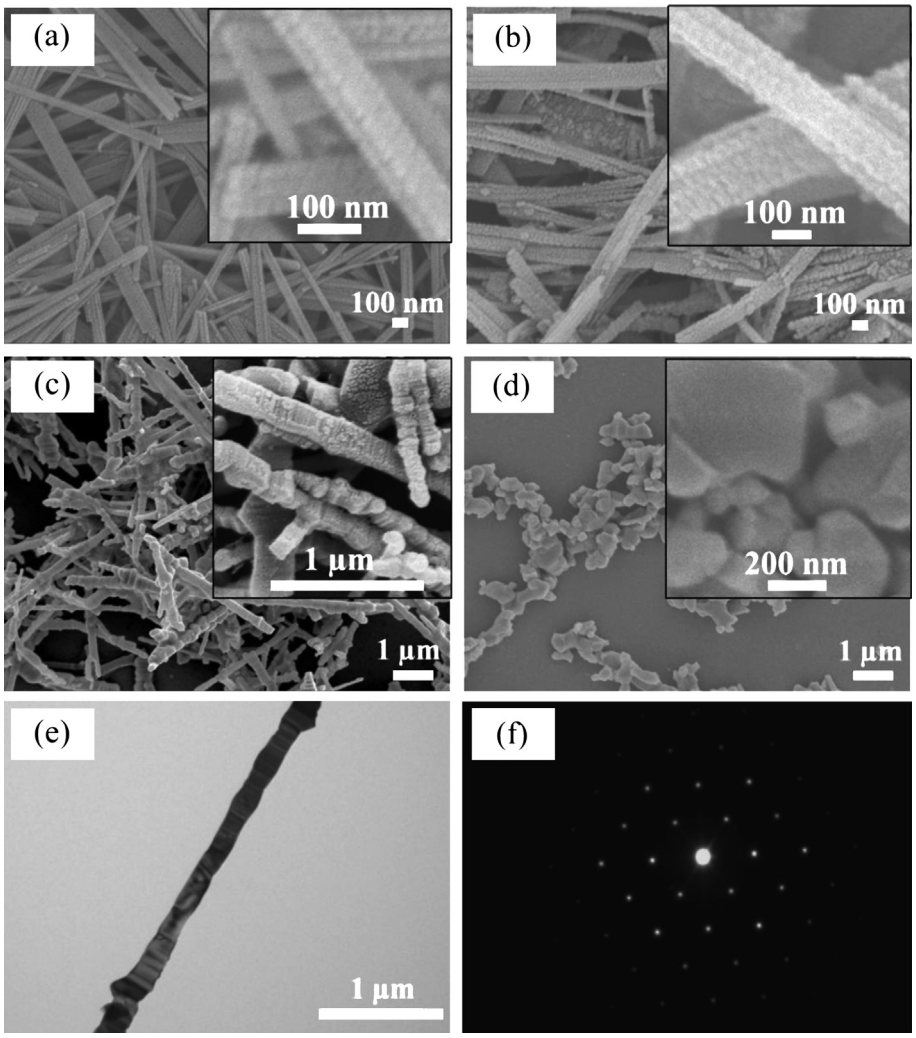


**Fig. 3.** The FESEM images of the (a) $Na_2TiO_3$ nanowires, (b) $Li_2TiO_3$ nanowires, (c) $Li_4Ti_5O_{12}$ nanorods and (d) $Li_4Ti_5O_{12}$ nanoparticles; (e) TEM image of $Li_4Ti_5O_{12}$ nanorods; (f) ED pattern of $Li_4Ti_5O_{12}$ nanorods.

collector and dried at 120 °C for 10 h in a vacuum oven. Then, Circular (1.6 $cm^2$) anode and cathode discs were individually punched from the copper and aluminum foil. The punched anodes and cathodes were respectively weighed to determine the amount of active materials about 1.5 and 3 mg before being loaded into coin-type cells. The cells were assembled in a glove box filled with high purity argon gas with low concentration of oxygen and low humidity. The electrolyte composed of 1 M $LiPF_6$ dissolved in ethylene carbonate (EC)/dimethyl carbonate (DMC) (1:1 in volume). Galvanostatic charge/discharge experiments were performed at different current densities (1 C rate corresponds to the current density of 175 mA $g^{-1}$ for $Li_4Ti_5O_{12}$ half cells and $Li_4Ti_5O_{12}$/$LiMn_2O_4$ full cells). Cyclic voltammetry (CV) and electrochemical impedance spectroscopy (EIS) were carried out using a Zahner IM6

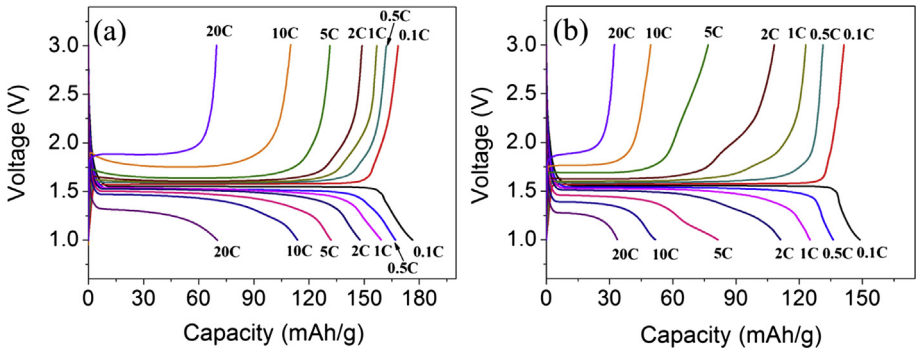


**Fig. 4.** Charge/discharge curves of $Li_4Ti_5O_{12}$ nanorods (a) and nanoparticles (b) at different rates.

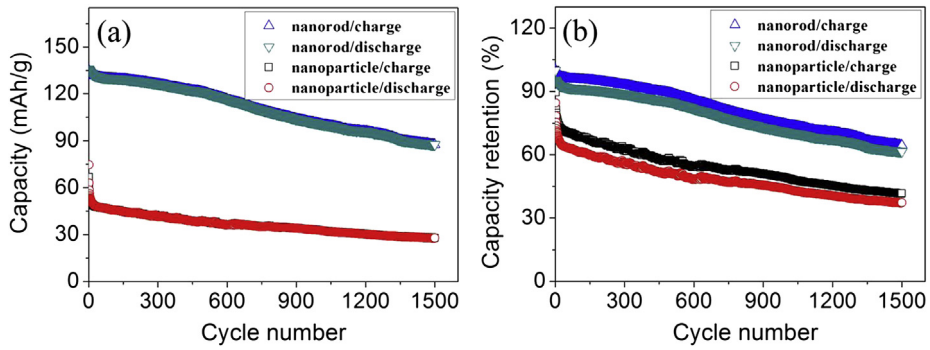


**Fig. 5.** The cycle performance (a) and capacity retention (b) of $Li_4Ti_5O_{12}$ nanorods and nanoparticles at 10 C rate.

electrochemical station. The sweep potential range of CV is between 1 and 2.2 V. The amplitude of the AC signal was 5 mV over the frequency range from 100 kHz to 0.01 Hz.

## 3. Results and discussion

### 3.1. Structure characterization of as-prepared powders

Fig. 2(a–b) shows XRD patterns of $Li_4Ti_5O_{12}$ nanorods, $Li_4Ti_5O_{12}$ nanoparticles, $Li_2TiO_3$ nanowires and $Na_2TiO_3$ nanowires, respectively. The peaks from Fig. 2(a) and (b) are indexed as the spinel structure $Li_4Ti_5O_{12}$ (JCPDS 49-0207). There is a very little peak at about 63.5° ($2\theta$) in Fig. 2(a), which belongs to $Li_2TiO_3$ phase, indicating little impurity. The peaks of $Li_4Ti_5O_{12}$ nanorods are sharper than that of $Li_4Ti_5O_{12}$ nanoparticles, revealing their better crystallinity. The XRD patterns from Fig. 2(c) and (d) are identical with the $Li_2TiO_3$ phase (JCPDS 33-0831) and $Na_2TiO_3$ phase (JCPDS 37-0346), respectively.

Fig. 3(a–d) shows the FESEM images of $Na_2TiO_3$ nanowires, $Li_2TiO_3$ nanowires, $Li_4Ti_5O_{12}$ nanorods and $Li_4Ti_5O_{12}$ nanoparticles, respectively. The average diameters of $Na_2TiO_3$ and $Li_2TiO_3$ nanowires are below 130 nm and the surface is rough. The average diameter of $Li_4Ti_5O_{12}$ nanorods is bigger than that of $Na_2TiO_3$ and $Li_2TiO_3$ nanowires and their surface becomes smoother. $Li_4Ti_5O_{12}$ nanoparticles have a strong tendency to form agglomerates, which are mainly made up of the particles with the size below 200 nm. From the inset of Fig. 3(d), it reveals that the aggregation of nanoparticles shows serious, and some big particles with the diameter about 300 nm were produced after aggregation. Moreover, the aggregation of $Li_4Ti_5O_{12}$ nanorods is slighter than nanoparticles. Fig. 3(e) and (f) present the TEM image and the electron diffraction (ED) pattern of $Li_4Ti_5O_{12}$ nanorods, which point out on their smooth surface and single-crystalline nature.

### 3.2. Electrochemical performance of Li/$Li_4Ti_5O_{12}$ half cells

Fig. 4(a) and (b) show charge/discharge properties of $Li_4Ti_5O_{12}$ nanorods and nanoparticles at different rates, respectively. From Fig. 4, it can see that the charge/discharge capacities of nanorods are higher than that of nanoparticles at various rates. The discharge

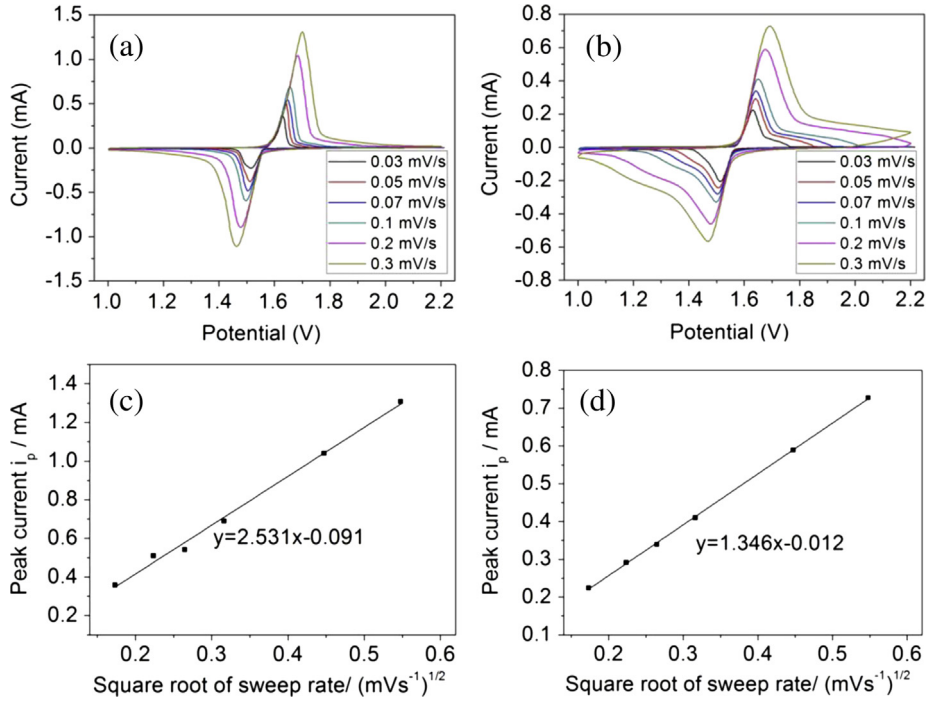


**Fig. 6.** Cyclic voltammograms of $Li_4Ti_5O_{12}$ nanorods (a) and nanoparticles (b) at different scan rates. Plotting of peak current (at around 1.66 V) vs. square root of the scan rate for $Li_4Ti_5O_{12}$ nanorods (c) and nanoparticles (d).

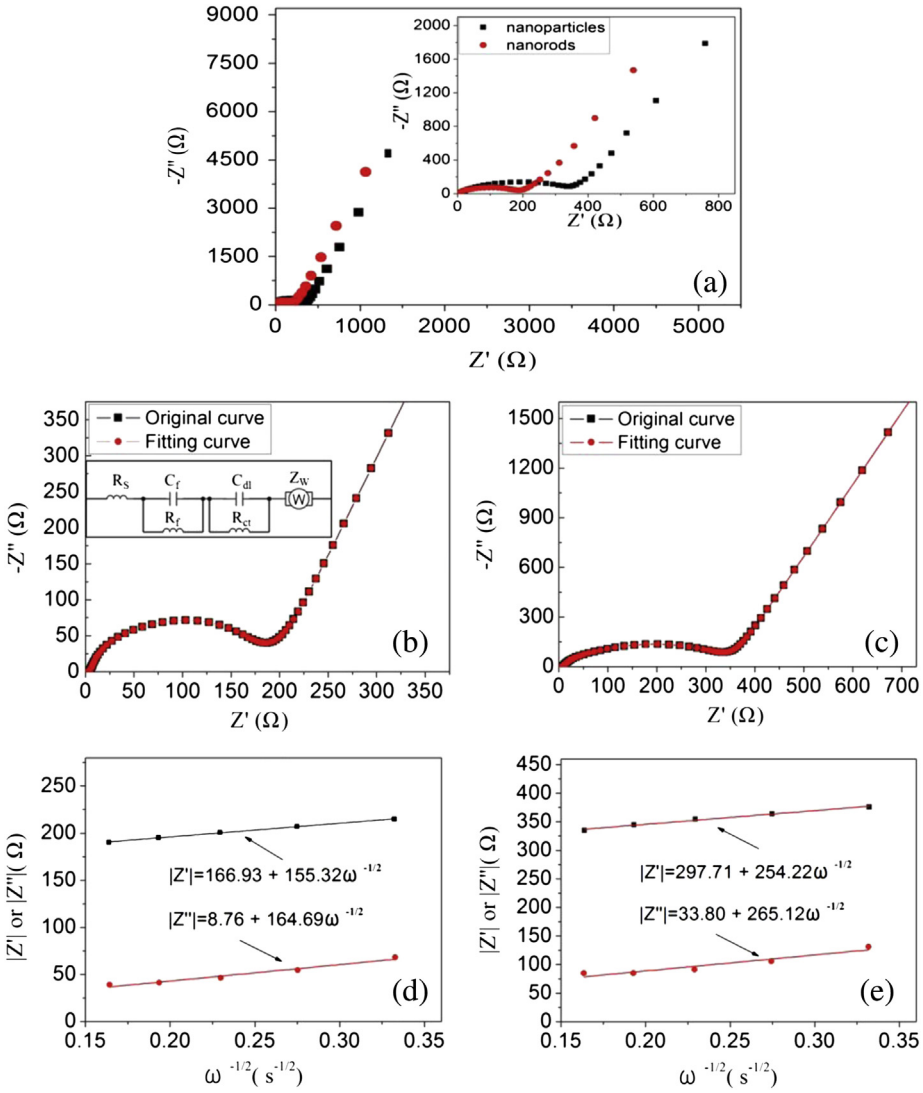


**Fig. 7.** (a) AC impedance of $Li_4Ti_5O_{12}$ nanorods and nanoparticles; (b–c) the AC impedance original curve and fitting curve for (b) nanorods and (c) nanoparticles; (d–e) the plotting of real resistance and imaginary resistance vs. inverse square root of the angular frequency for (d) nanorods; (e) nanoparticles.

capacity of nanorods is up to 176.4 mAh $g^{-1}$ at 0.1 C rate, while the discharge capacity of nanoparticles is only 148.8 mAh $g^{-1}$. Remarkably, the discharge capacities of nanorods with the values of 113.7 and 69.7 mAh $g^{-1}$ are far greater than that of nanoparticles with values of 51.7 and 33.7 mAh $g^{-1}$ at 10 C and 20 C rates, respectively, which reveals that single crystalline $Li_4Ti_5O_{12}$ nanorods displays better rate capability.

Fig. 5 reveals the cycle performance and capacity retention of $Li_4Ti_5O_{12}$ nanorods and nanoparticles at 10 C rate. Again, $Li_4Ti_5O_{12}$ nanorods display higher capacity and better cycle stability. The first discharge capacity of nanorods is about 135.9 mAh $g^{-1}$ at 10 C rate, and the capacity retention is more than 61.5% after 1500 cycles, compared to the first discharge capacity of nanoparticles of 74.6 mAh $g^{-1}$ at 10 C rate, and the capacity retention of only 37.3% after 1500 cycles.

Fig. 6(a) and (b) show cyclic voltammograms of $Li_4Ti_5O_{12}$ nanorods and nanoparticles at different scan rates, which reveal that the peak current increases with the increase of scan rates. Moreover, the peak current of $Li_4Ti_5O_{12}$ nanorods is higher than of nanoparticles at the same scan rate, which implies that the internal resistance of $Li_4Ti_5O_{12}$ nanorods anode is smaller than that of nanoparticles and the diffusion rate of $Li^+$ is faster. In Fig. 6(c) and (d), the plots of the peak currents vs. the square root of the scan rates of both nanorods and nanoparticles show linear relationship, which suggests that lithium insertion in $Li_4Ti_5O_{12}$ powders is a diffusion-controlled process. For a reversible reaction involving Li-ion diffusion behavior, the chemical diffusion coefficient of $Li^+$ ions can be obtained by the Randles–Sevcik equation [55]:

$$i_p = 0.4463 z^{3/2} F^{3/2} C_{Li} A R^{-1/2} T^{-1/2} D_{Li}^{1/2} v^{1/2} \quad (1)$$

where $i_p$ being the peak current value (A), $z$ being the charge transfer number ( for lithium ion $z = 1$), $F$ being the Faraday's

**Table 1**
Impedance parameters of equipment circuit of $Li_4Ti_5O_{12}$ nanorods and nanoparticles electrodes.

| Sample | $R_s$ (Ω) | $R_f$ (Ω) | $R_{ct}$ (Ω) | $A_r$ | $A_i$ | $\sigma$ |
|---|---|---|---|---|---|---|
| Nanorods | 3.02 | 50.51 | 92.20 | 155.32 | 164.69 | 160.01 |
| Nanoparticles | 6.51 | 60.69 | 197.10 | 254.22 | 265.12 | 259.67 |

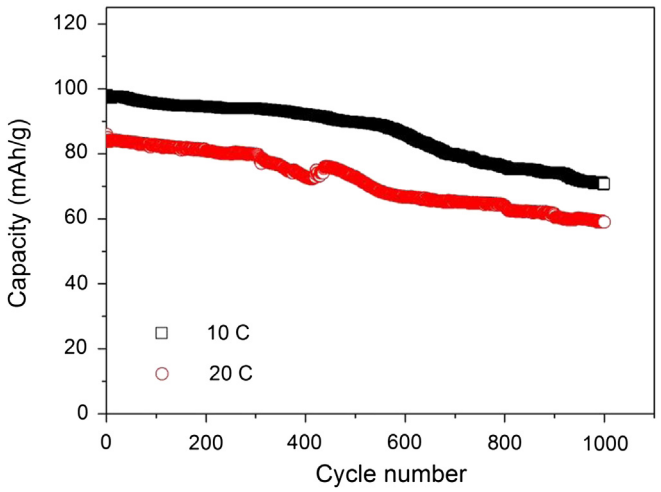


**Fig. 8.** The cycle performance of $LiMn_2O_4$ porous sphere at 10 C and 20 C rates.

constant (96485 C $mol^{-1}$), $C_{Li}$ being the Li-ion concentration (0.08747 mol $cm^{-3}$), $A$ being the surface area of electrode ($cm^2$), $R$ being the universal gas constant (8.314 J $mol^{-1}$ $K^{-1}$), $T$ being the absolute temperature (K), $D_{Li}$ being the chemical diffusion coefficient ($cm^2$ $s^{-1}$), and $v$ being the scanning rate (V $s^{-1}$). The anodic chemical diffusion coefficients of $Li^+$ ions in $Li_4Ti_5O_{12}$ nanorods and nanoparticles electrodes calculated by equation (1) from the slope of $i_p$ vs. $v^{1/2}$ plot are $4.53 \times 10^{-9}$ and $1.28 \times 10^{-9}$ $cm^2$ $s^{-1}$, respectively. The single-crystalline $Li_4Ti_5O_{12}$ nanorods electrode reveals larger chemical diffusion coefficient, which demonstrates that $Li_4Ti_5O_{12}$ nanorods is more favorable for lithium ion diffusion, and can partly illustrate the reason for $Li_4Ti_5O_{12}$ nanorods displaying higher rate capability.

Fig. 7 shows the AC impedance spectra of batteries after activation. The impedance spectra composed of two depressed semicircles in high-to-medium frequency region and a straight line in low frequency region. In high frequency region, an intercept at the $Z_{real}$ axis corresponds to the ohmic resistance ($R_s$) and the semicircle correlates closely to the Li-ion migration resistance ($R_f$) through the multilayer surface films. The semicircle in the middle frequency range is related to the charge transfer resistance ($R_{ct}$) and the inclined line at low frequency region represents the Warburg impedance ($Z_\omega$), which is associated with lithium-ion diffusion in the $Li_4Ti_5O_{12}$ particles. The parameters of impedance spectra were simulated by Zview software and the spectra have been fitted to an equivalent circuit shown in the inset of Fig. 7(b). The parameter results were listed in Table 1. From Table 1, it can be seen that the as-assembled cell for $Li_4Ti_5O_{12}$ nanorods reveals smaller $R_s$, $R_f$ and $R_{ct}$ with the values of 3.02, 50.51 and 92.20 Ω than $Li_4Ti_5O_{12}$ nanoparticles with the values of 6.51, 60.69 and 197.10 Ω, respectively. Especially, the difference of $R_{ct}$ is very large between $Li_4Ti_5O_{12}$ nanorods and nanoparticles. It can partly state the reason for $Li_4Ti_5O_{12}$ nanorods revealing better rate capability than nanoparticles. The Warburg coefficients ($\sigma$) can be considered as a resistance barrier for lithium ion diffusion because it is inversely proportion to the diffusion coefficient of lithium ion in electrode. The conventional Warburg impedance ($Z_\omega$) formula [56] is shown as follows:

$$Z_\omega = \sigma(1-j)\omega^{-1/2}, \left|Z'\right| = A_r\omega^{-1/2}, \left|Z''\right| = A_i\omega^{-1/2}, \quad \sigma = (A_r + A_i)/2 \tag{2}$$

where $\sigma$ being the Warburg coefficient, $j$ being the square root of −1, $\omega$ being the angular frequency, $|Z'|$ being the real resistance, $|Z''|$ being the imaginary resistance, $A_r$ being the Warburg coefficient of real part and $A_i$ being the Warburg coefficient of imaginary part. According to the formula, the Warburg coefficient of real part and imaginary part can be obtained from the slope of the $|Z'|$ vs. $\omega^{-1/2}$ and $|Z''|$ vs. $\omega^{-1/2}$, respectively. Fig. 7(d–e) reveals the linear relationship of $|Z'|$ vs. $\omega^{-1/2}$ and $|Z''|$ vs. $\omega^{-1/2}$ for $Li_4Ti_5O_{12}$ nanorods

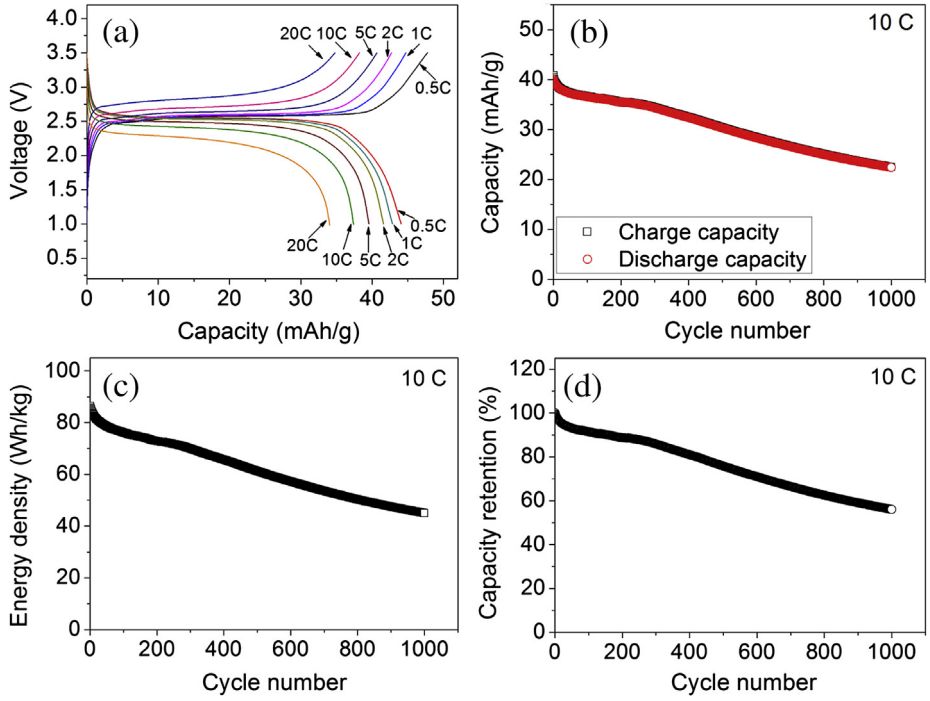


**Fig. 9.** Electrochemical performances of $Li_4Ti_5O_{12}/LiMn_2O_4$ full cells at room temperature: (a) charge/discharge capacities at different rates; (b) cycle performance; (c) energy density and (d) capacity retention.

and nanoparticles cells. The $A_r$ ($A_i$) in $Li_4Ti_5O_{12}$ nanorods and nanoparticles electrodes are separately 155.32 (164.69) and 254.22 (265.12), which were calculated by the equation (2) with the slope of the $|Z'|$ vs. $\omega^{-1/2}$ and $|Z''|$ vs. $\omega^{-1/2}$ plot are listed in Table 1. Moreover, Warburg coefficients ($\sigma$) were also calculated in $Li_4Ti_5O_{12}$ nanorods and nanoparticles electrodes with the values of 160.01 and 259.67, respectively, which displays that the as-assembled cell for $Li_4Ti_5O_{12}$ nanorods shows smaller Warburg coefficient which further confirms that $Li_4Ti_5O_{12}$ nanorods is more suitable for lithium ion diffusion. This result is extremely coincident with the lithium-ion diffusion coefficient obtained through cyclic voltammetry.

### 3.3. Electrochemical performance of Li/$LiMn_2O_4$ half cells

Spinel $LiMn_2O_4$ is generally considered as excellent alternative to $LiCoO_2$ in power LIBs because it is inexpensive, safe and environmentally friendly [57,58]. Fig. 8 shows the cycle performance of $LiMn_2O_4$ porous spheres at 10 C and 20 C rates. The first discharge capacities are up to 98.1 and 85.9 mAh $g^{-1}$ at 10 C and 20 C rates, and after 1000 cycles, the corresponding retention rates of capacities are more than 72% and 68% at room temperature. The detailed information concerning this material can be found in our previous report [54].

### 3.4. Electrochemical performances of $Li_4Ti_5O_{12}$/$LiMn_2O_4$ full cells

Fig. 9(a) shows charge/discharge curves of $Li_4Ti_5O_{12}$/$LiMn_2O_4$ full cells at different rates, while Fig. 9(b–d) shows the cycle property of the cell at 10 C rate. From Fig. 9(a), discharge capacities of the cell are individually 44.1, 42.9, 41.6, 39.6, 37.4, 34.1 mAh $g^{-1}$ at 0.5 C, 1 C, 2 C, 5 C, 10 C and 20 C, which are calculated through basing on the total weight of both active electrode materials. The capacity ratios of 10 C and 20 C–0.5 C are separately 84.8% and 77.3%, suggesting excellent high rate capability. Moreover, the output voltage of the cell is approximately 2.5 V. From Fig. 9(c), the mass energy density of the cell is up to 86.4 Wh $kg^{-1}$ at 10 C rate. In Fig. 9(d), it reveals the capacity retention of the cell being about 60% after 1000 cycles at 10 C rate, indicating superior cycle stability.

## 4. Conclusions

Single-crystalline $Li_4Ti_5O_{12}$ nanorods with excellent electrochemical performance have been successfully synthesized through a molten salt method, followed by a precipitation method. The single-crystalline $Li_4Ti_5O_{12}$ nanorods electrode reveals higher capacity, better cycle performance and faster lithium ion diffusion than that of $Li_4Ti_5O_{12}$ nanoparticles. The first discharge capacity of $Li_4Ti_5O_{12}$ nanorods is up to 135.9 mAh $g^{-1}$ at 10 C rate and the capacity retention is more than 61.5% after 1500 cycles. High rate capability $Li_4Ti_5O_{12}$/$LiMn_2O_4$ full cell is demonstrated with the discharge capacity and mass energy density reaching 40 mAh $g^{-1}$ and 86.4 Wh $kg^{-1}$ at 10 C rate. Its capacity retention is about 60% after 1000 cycles, suggesting the $Li_4Ti_5O_{12}$/$LiMn_2O_4$ full cells as promising candidates for the power of hybrid electric vehicles.

## Acknowledgments

This work was financially supported by the HKSAR RGC grant (GRF project CityU 100510, #9041528).

## References

[1] M. Wagemaker, E.R.H. van Eck, A.P.M. Kentgens, F.M. Mulder, J. Phys. Chem. B 113 (2009) 224–230.
[2] F. Ronci, P. Reale, B. Scrosati, S. Panero, V.R. Albertini, P. Perfetti, M. Michiel, J.M. Merino, J. Phys. Chem. B 106 (2002) 3082–3086.
[3] D.T. Liu, C.Y. Ouyang, J. Shu, J. Jiang, Z.X. Wang, L.Q. Chen, Phys. Status Solidi B 243 (2006) 1835–1841.
[4] J.X. Ma, C.S. Wang, S. Wroblewski, J. Power Sources 164 (2007) 849–856.
[5] L. Cheng, X.L. Li, H.J. Liu, H.M. Xiong, P.W. Zhang, Y.Y. Xia, J. Electrochem. Soc. 154 (2007) A692–A697.
[6] J.-W. Shin, J.H. Ryu, J. Jeong, D.-H. Yoon, J. Electroceram. 28 (2012) 178–184.
[7] Z.M. Liu, N.Q. Zhang, Z.J. Wang, K.N. Sun, J. Power Sources 205 (2012) 479–482.
[8] J. Lu, C.Y. Nan, Q. Peng, Y.D. Li, J. Power Sources 202 (2012) 246–252.
[9] J.Z. Chen, L. Yang, S.H. Fang, S. Hirano, K. Tachibana, J. Power Sources 200 (2012) 59–66.
[10] H.L. Wu, Y.D. Huang, D.Z. Jia, Z.P. Guo, M. Miao, J. Nanopart Res. 14 (2012) 713.
[11] A. Laumann, M. Bremholm, P. Hald, M. Holzapfel, K.T. Fehr, B.B. Iversen, J. Electrochem. Soc. 159 (2012) A166–A171.
[12] N.Q. Zhang, Z.M. Liu, T.Y. Yang, C.L. Liao, Z.J. Wang, K.N. Sun, Electrochem. Commun. 13 (2011) 654–656.
[13] S.-H. Yu, A. Pucci, T. Herntrich, M.-G. Willinger, S.-H. Baek, Y.-E. Sung, N. Pinna, J. Mater. Chem. 21 (2011) 806–810.
[14] J. Lim, E. Choi, V. Mathew, D. Kim, D. Ahn, J. Gim, S.-H. Kang, J. Kim, J. Electrochem. Soc. 158 (2011) A275–A280.
[15] A.S. Prakash, P. Manikandan, K. Ramesha, M. Sathiya, J.-M. Tarascon, A.K. Shukla, Chem. Mater. 22 (2010) 2857–2863.
[16] D. Wang, N. Ding, X.H. Song, C.H. Chen, J. Mater. Sci. 44 (2009) 198–203.
[17] J. Li, Y.-L. Jin, X.-G. Zhang, H. Yang, Solid State Ionics 178 (2007) 1590–1594.
[18] D.H. Kim, Y.S. Ahn, J. Kim, Electrochem. Commun. 7 (2005) 1340–1344.
[19] J. Wang, X.-M. Liu, H. Yang, Trans. Nonferrous Met. Soc. China 22 (2012) 613–620.
[20] R. Cai, S.M. Jiang, X. Yu, B.T. Zhao, H.T. Wang, Z.P. Shao, J. Mater. Chem. 22 (2012) 8013–8021.
[21] B. Zhang, Z.-D. Huang, S.W. Oh, J.-K. Kim, J. Power Sources 196 (2011) 10692–10697.
[22] Y.-R. Jhan, C.-Y. Lin, J.-G. Duh, Mater. Lett. 65 (2011) 2502–2505.
[23] Z.H. Wang, G. Chen, J. Xu, Z.S. Lv, W.Q. Yang, J. Phys. Chem. Solids 72 (2011) 773–778.
[24] S.Z. Ji, J.Y. Zhang, W.W. Wang, Y. Huang, Z.R. Feng, Z.T. Zhang, Z.L. Tang, Mater. Chem. Phys. 123 (2010) 510–515.
[25] J. Wolfenstine, J.L. Allen, J. Power Sources 180 (2008) 582–585.
[26] Y.D. Huang, Y.L. Qi, D.Z. Jia, X.C. Wang, Z.P. Guo, W. Cho II, J. Solid State Electrochem. 16 (2012) 2011–2016.
[27] L. Cheng, J. Yan, G.-N. Zhu, J.-Y. Luo, C.-X. Wang, Y.-Y. Xia, J. Mater. Chem. 20 (2010) 595–602.
[28] M.-L. Lee, Y.-H. Li, S.-C. Liao, J.-M. Chen, J.-W. Yeh, H.C. Shih, Appl. Surf. Sci. 258 (2012) 5938–5942.
[29] J.X. Tang, L.J. Gao, Phys. Scr. 85 (2012) 045802.
[30] C.-T. Hsieh, B.-S. Chang, J.-Y. Lin, R.-S. Juang, J. Alloys Compd. 513 (2012) 393–398.
[31] H.L. Pan, L. Zhao, Y.-S. Hu, H. Li, L.Q. Chen, ChemSusChem 5 (2012) 526–529.
[32] E. Kang, Y.S. Jung, G.-H. Kim, J. Chun, U. Wiesner, A.C. Dillon, J.K. Kim, J. Lee, Adv. Funct. Mater. 21 (2011) 4349–4357.
[33] H.-G. Jung, J. Kim, B. Scrosati, Y.-K. Sun, J. Power Sources 196 (2011) 7763–7766.
[34] H.-G. Jung, S.-T. Myung, C.S. Yoon, S.-B. Son, K.H. Oh, K. Amine, B. Scrosati, Y.-K. Sun, Energy Environ. Sci. 4 (2011) 1345–1351.
[35] L. Zhao, Y.-S. Hu, H. Li, Z.X. Wang, L.Q. Chen, Adv. Mater. 23 (2011) 1385–1388.
[36] J. Wang, X.-M. Liu, H. Yang, X.-D. Shen, J. Alloys Compd. 509 (2011) 712–718.
[37] Y.-B. He, F. Ning, B.H. Li, Q.-S. Song, W. Lv, H.D. Du, D.Y. Zhai, F.Y. Su, Q.-H. Yang, F.Y. Kang, J. Power Sources 202 (2012) 253–261.
[38] S.C. Lee, S.M. Lee, J.W. Lee, J.B. Lee, S.M. Lee, S.S. Han, H.C. Lee, H.J. Kim, J. Phys. Chem. C 113 (2009) 18420–18423.
[39] J. Kim, J. Cho, Electrochem. Solid-State Lett. 10 (2007) A81–A84.
[40] C. Lai, Y.Y. Dou, X. Li, X.P. Gao, J. Power Sources 195 (2010) 3676–3679.
[41] Y.F. Tang, L. Yang, Z. Qiu, J.S. Huang, Electrochem. Commun. 10 (2008) 1513–1516.
[42] Y. Li, G.L. Pan, J.W. Liu, X.P. Gao, J. Electrochem. Soc. 156 (2009) A495–A499.
[43] H.-K. Kim, S.-M. Bak, K.-B. Kim, Electrochem. Commun. 12 (2010) 1768–1771.
[44] H.-W. Lu, W. Zeng, Y.-S. Li, Z.-W. Fu, J. Power Sources 164 (2007) 874–879.
[45] C.H. Jiang, Y. Zhou, I. Honma, T. Kudo, H.S. Zhou, J. Power Sources 166 (2007) 514–518.
[46] N.D. He, B.S. Wang, J.J. Huang, J. Solid State Electrochem. 14 (2010) 1241–1246.
[47] Y.-S. Lin, J.-G. Duh, J. Power Sources 196 (2011) 10698–10703.
[48] Y.F. Tang, L. Yang, Z. Qiu, J.S. Huang, J. Mater. Chem. 19 (2009) 5980–5984.
[49] Y. Lv, H. Zhang, G.P. Cao, B.Y. Wang, X.D. Wang, Mater. Res. Bull. 46 (2011) 2312–2316.
[50] L.F. Shen, C.Z. Yuan, H.J. Luo, X.G. Zhang, L. Chen, H.S. Li, J. Mater. Chem. 21 (2011) 14414–14416.
[51] L.F. Shen, C.Z. Yuan, H.J. Luo, X.G. Zhang, K. Xu, Y.Y. Xia, J. Mater. Chem. 20 (2010) 6998–7004.

[52] C.C. Li, Q.H. Li, L.B. Chen, T.H. Wang, ACS Appl. Mater. Interfaces 4 (2012) 1233–1238.
[53] T. Kasuga, M. Hiramatsu, A. Hoson, T. Sekino, K. Niihara, Langmuir 14 (1998) 3160–3163.
[54] L.J. Xi, H.-E. Wang, Z.G. Lu, S.L. Yang, R.G. Ma, J.Q. Deng, C.Y. Chung, J. Power Sources 198 (2012) 251–257.
[55] J. Xie, N. Imanishi, A. Hirano, M. Matsumura, Y. Takeda, O. Yamamoto, Solid State Ionics 178 (2007) 1218–1224.
[56] R. Greef, R. Peat, L.M. Peter, et al., Instrumental Methods in Electrochemistry, John Wiley &Sons, Inc., New York, 1986, p. 265.
[57] P.G. Bruce, B. Scrosati, J.M. Tarascon, Angew. Chem. Int. Ed. 47 (2008) 2930–2946.
[58] G. Amatucci, J.M. Tarascon, J. Electrochem. Soc. 149 (2002) K31–K46.